

The Sign-Switching of the Cosmological Constant

Mariam Bouhmadi-López^{a,b,c,*} and Beñat Ibarra-Uriondo^{b,c}

^a*IKERBASQUE, Basque Foundation for Science, 48011, Bilbao, Spain*

^b*Department of Physics, University of the Basque Country UPV/EHU, P.O. Box 644, 48080 Bilbao, Spain*

^c*EHU Quantum Center, University of the Basque Country UPV/EHU, P.O. Box 644, 48080 Bilbao, Spain*

E-mail: mariam.bouhmadi@ehu.eus, benat.ibarra@ehu.eus

We propose and investigate a class of dynamical dark energy models in which the cosmological constant evolves from negative values in the early Universe to a positive value at low redshifts. This framework includes a generalised ladder-step evolution, as well as smooth-transition scenarios, providing a unified description of sign-changing cosmological constants. We analyse the theoretical construction and background dynamics of these models using cosmographic diagnostics. Extending this study to the linear perturbation regime, we solve the perturbation equations from the radiation-dominated era with adiabatic initial conditions. We examine the evolution of the matter density contrast, gravitational potential, and the $f\sigma_8$ observable. Our results are compared against the standard Λ CDM model and confronted with current observational data, illustrating the phenomenological viability of sign-changing dark energy models and revealing distinctive imprints on cosmic structure formation arising from the transition of the cosmological constant.

Proceedings of the Corfu Summer Institute 2025 "School and Workshops on Elementary Particle Physics and Gravity" (CORFU2025) 2 - 8 September, 2025 Corfu, Greece

*Speaker

© Copyright owned by the author(s) under the terms of the Creative Commons Attribution-NonCommercial-NoDerivatives 4.0 International License (CC BY-NC-ND 4.0). All rights for text and data mining, AI training, and similar technologies for commercial purposes, are reserved. ISSN 1824-8039. Published by SISSA Medialab.

<https://pos.sissa.it/>

1. Introduction

The late-time accelerated expansion of the Universe, first observed through Type Ia supernovae [1], is well described by the concordance Λ CDM model. However, persistent tensions in key cosmological parameters, most notably the H_0 and S_8 discrepancies [2–6], motivate the exploration of minimal extensions to the standard framework.

A wide range of theoretical extensions beyond the standard cosmological model have been proposed to address the current observational tensions, aiming to reconcile data while preserving the well-established successes of Λ CDM in describing both early- and late-time cosmic evolution [7, 8]. Broadly speaking, these proposals can be organised into two main directions.

The first focuses on alternative dark energy (DE) frameworks in which the cosmological constant is replaced by a dynamical component. Within this class, one can distinguish between early-time and late-time modifications. Early-time scenarios include, for instance, Early Dark Energy (EDE) [3], Anti-de Sitter Early Dark Energy (AdS-EDE) [9–11], and New Early Dark Energy (NEDE) [12–14]. Late-time realisations instead modify the recent expansion history, often through changes in the effective DE density or equation of state (EoS). Representative examples are phantom-crossing DE models [15–17], the Omnipotent DE scenario [16, 18], (non-minimally) interacting DE models [19–21], and axion-like DE constructions [22–24].

The second major avenue involves modifications of general relativity itself. In this approach, cosmic acceleration is not attributed to an additional energy component but rather to departures from Einstein's theory on cosmological scales. Well-studied examples include $f(\mathcal{R})$ gravity [25–28], $f(\mathcal{T})$ gravity [29–32], $f(\mathcal{R}, T)$ models [33, 34], and $f(Q)$ theories [35–39]. Additional frameworks include bimetric gravity [40] and kinetic gravity braiding (KGB) scenarios [41–44], among many others.

From the first type we have a particularly promising alternative, the Λ_s CDM model [45–60], inspired by the graduated dark energy scenario [61]. In this framework, the cosmological constant is replaced by an effective dark energy density that undergoes a transition from negative (AdS-like) to positive (dS-like) values at low redshift, $z = z_\dagger \lesssim 2$. This late-time modification leaves early-Universe physics unaffected while significantly alleviating the H_0 and S_8 tensions [47, 55]. Interestingly, the presence of a negative cosmological constant is theoretically appealing, as AdS vacua naturally arise in string-theoretic and holographic settings [62].

The simplest realisation of Λ_s CDM assumes an abrupt sign switch, typically modelled by a signum function. While phenomenologically successful, this instantaneous transition introduces a discontinuity in the cosmological constant at $z = z_\dagger$, leading to a type II (sudden) singularity [63]. Although such a singularity has been shown to have a negligible impact on the evolution of cosmic structures [48], it nevertheless indicates that the abrupt model should be regarded as an idealised approximation to a more realistic scenario in which the transition is very rapid but smooth, as in graduated dark energy [61], while also implementing a finite DE component in the past.

Motivated by this, we have proposed several smooth extensions of the abrupt Λ_s CDM model [64] (see also [49–52] for alternative smooth behaviours). These include models featuring a ladder-like cosmological constant, a smooth step function, and an error-function profile. By construction, these scenarios eliminate sudden singularities, replacing them with milder w -singularities, while preserving the successful background evolution of the original model. Importantly, these smooth

transitions allow for a consistent perturbative treatment, enabling the study of structure formation through linear perturbation theory.

The impact of these models on the growth of matter perturbations can be directly tested using large-scale structure observables such as the growth rate $f\sigma_8$ and the matter power spectrum. Preliminary analyses indicate that smooth sign-switching models remain compatible with current observational data while providing a more physically motivated description of late-time DE dynamics.

This manuscript is based on our work [64, 65] and is organised as follows. In Sec. 2 we introduce and compare the abrupt sign-switching model with its three smoother extensions. In Sec. 3 we present the evolution of the cosmographic parameters of these models. In Sec. 4 we examine the evolution of linear matter perturbations, the gravitational potential, and structure formation using several measurements of the growth rate function, specifically $f\sigma_8$. We conclude briefly in Sec. 5.

2. Beyond the standard model

In this section, we introduce and compare the abrupt sign-switching model with three smoother extensions. We present the phenomenological evolution of each dark energy (DE) density in turn. Our analysis is carried out within the standard framework of a homogeneous and isotropic cosmological background described by the Friedmann–Lemaître–Robertson–Walker (FLRW) line element. We restrict attention to a spatially flat geometry and model the cosmic energy content as a set of non-interacting components: radiation, pressureless matter — comprising both baryonic and cold dark matter contributions — and DE.

2.1 Abrupt sign-switching model (Λ_s CDM) – Model (A)

We start by considering the most elementary realisation of a sign-changing DE model, namely Λ_s CDM [45]. This single-parameter extension of Λ CDM is characterised by a DE density that transitions from a constant negative value to a constant positive one via a step function, namely,

$$\Lambda_s(z) = \Lambda \operatorname{sgn}(z_{\dagger,s} - z), \quad (1)$$

where $z_{\dagger,s}$ denotes the redshift at which the sign-switching occurs, and Λ represents the present-day value of the cosmological constant, at which the model reduces to the well-known Λ CDM scenario. The function $\operatorname{sgn}(z_{\dagger,s} - z)$ represents the signum function, taking the value 1 when its argument is positive and -1 when it is negative. The EoS parameter remains constant at all times, mimicking Λ CDM except at the sign-switching, when it diverges,

$$w_{d,s} = -1 - \frac{\delta(z_{\dagger,s} - z)}{3 \operatorname{sgn}(z_{\dagger,s} - z)} (1 + z). \quad (2)$$

Here $\delta(z_{\dagger,s} - z)$ stands for the Dirac delta function. It follows that the EoS parameter becomes undefined at the moment of the sign change, giving rise to a singular behaviour that was analysed in [48]. Additional details of this model can be found in Ref. [45].

2.2 Ladder-like DE model ($\Lambda\Lambda\text{CDM}$) – Model (B)

This framework represents a natural generalisation of the previous case, extending from a single step to N successive steps. Each step introduces a discrete increase in the DE density via a “small” discontinuous function. The size of each step is determined by the total number of steps, and for simplicity, all steps are taken to be equal. Throughout this work, we fix $N = 20$, thereby rendering the model effectively a two-parameter extension of ΛCDM , defined by an initial and final redshift, $z_{i,le}$ and $z_{f,le}$, which mark the beginning and end of the transition from $-\Lambda$ to $+\Lambda$. The growth of the cosmological constant is encoded through an N -step ladder function, with the length of each step serving as a controllable parameter

$$\Lambda_l(z) = \Lambda \left[1 - \frac{2}{N} \sum_{n=1}^N \mathcal{H}(z_n - z) \right]. \quad (3)$$

The redshift at which each step transition occurs is given by

$$\begin{aligned} z_n &= z_{f,l} + \frac{n}{N} (z_{i,l} - z_{f,l}), \\ z_{i,l} &= z_{\dagger,l} + \Delta z \cdot \frac{N}{2}, \\ z_{f,l} &= z_{\dagger,l} - \Delta z \cdot \frac{N}{2}, \end{aligned} \quad (4)$$

where $n \in [0, N]$ indexes the steps, ordered from the present to the past, $z_{\dagger,l}$ is the sign-switching redshift and Δz the length of each step. The function $\mathcal{H}(z_n - z)$ denotes the Heaviside step function evaluated at $z_n - z$. As in the simpler single-step case, the EoS parameter exhibits singularities at each discontinuity corresponding to the step transitions:

$$w_{d,l} = -1 - \frac{(1+z) \sum_{i=1}^N \delta(z_n - z)}{3 \left[-N/2 + \sum_{n=1}^N \mathcal{H}(z_n - z) \right]}. \quad (5)$$

In this model, the EoS parameter remains -1 throughout all regimes, except at the locations of the step transitions, where it diverges owing to the presence of Dirac delta functions.

2.3 SSCDM – Model (C)

The third model represents another two-parameter extension of ΛCDM , in which the DE density evolves smoothly from negative to positive values over a specified redshift range through an interpolation polynomial. The additional parameters are the redshift at which the transition commences, $z_{i,ss}$, and the redshift at which it concludes, $z_{f,ss}$; these parameters control the smoothness of the transition. Within this framework, the DE density is expressed as:

$$\Lambda_{ss}(x) = \Lambda \begin{cases} -1, & x \leq x_{i,ss}, \\ 1 - 2(126t^5 - 420t^6 + 540t^7 - 315t^8 + 70t^9), & x_{i,ss} < x < x_{f,ss}, \\ 1, & x \geq x_{f,ss}, \end{cases} \quad (6)$$

where

$$t = \frac{x - x_{f,ss}}{x_{i,ss} - x_{f,ss}}, \quad x = -\ln(1+z).$$

In these class of models, the EoS parameter departs from the Λ CDM behaviour, since the DE density is no longer constant over part of the cosmic evolution. Consequently, the EoS parameter becomes time-dependent and evolves as

$$w_{d,ss}(x) = \begin{cases} -1, & x \leq x_{i,ss}, \\ -1 - \frac{1260}{\Delta x \Lambda_{ss}(x)/\Lambda} (t^4 - 4t^5 + 6t^6 - 4t^7 + t^8), & x_{i,ss} < x < x_{f,ss}, \\ -1, & x \geq x_{f,ss}, \end{cases} \quad (7)$$

where $\Delta x = x_{i,ss} - x_{f,ss}$. In models (A) and (B), the EoS parameter contains Dirac delta contributions at each step discontinuity, originating from the derivative of the step function. This behaviour is absent in the present model, as the transition in the DE density is implemented in a smooth manner.

Nevertheless, as is generic in DE models featuring a transition from negative to positive energy density, the EoS parameter $w_{d,ss}(x)$ diverges at the point where the sign change occurs, undergoing a crossing of the cosmological constant line, $w = -1$, through infinite values. Although $w_{d,ss}(x)$ is not well defined over the entire interval $x \in (x_{i,ss}, x_{f,ss})$, the total equation-of-state parameter, $w_{\text{tot}} = \Omega_r/3 + w_d\Omega_d$, where Ω_r and Ω_d denote the radiation and DE fractional energy densities, respectively, remains well behaved throughout the evolution.

2.4 ECDM – Model (D)

In this model, we introduce a DE density that evolves according to an interpolating error function¹. Specifically, we assume

$$\Lambda_e(x) = \Lambda \operatorname{erf}[\eta (x - x_{\dagger,e})], \quad (8)$$

where η is a parameter controlling the smoothness of the transition, and $x_{\dagger,e} = -\ln(1 + z_{\dagger,e})$ denotes the redshift at which the DE density changes sign. This construction therefore constitutes a two-parameter extension of the standard Λ CDM framework.

The corresponding EoS parameter can be straightforwardly derived by enforcing conservation of the DE energy-momentum tensor, yielding

$$w_{d,e}(x) = -1 - \frac{2\eta e^{-\eta^2(x-x_{\dagger,e})^2}}{3\sqrt{\pi} \operatorname{erf}[\eta (x - x_{\dagger,e})]}. \quad (9)$$

As in model (C), the smooth evolution of the DE density in this scenario removes the Dirac delta contributions to the EoS parameter that are present in models (A) and (B). Nonetheless, similarly to the previous case, the vanishing of the error function at the sign-changing point $x = x_{\dagger,e}$ causes the EoS parameter to diverge, resulting in a cosmological constant line crossing through infinite values. By contrast, the total EoS parameter, $w_{\text{tot}} = \Omega_r/3 + w_d\Omega_d$, remains well defined, exhibiting a regular background evolution throughout.

¹The error function is a function $\operatorname{erf}: \mathbb{C} \rightarrow \mathbb{C}$ defined as:

$$\operatorname{erf}(z) = \frac{2}{\sqrt{\pi}} \int_0^z e^{-t^2} dt.$$

2.5 Model comparison

A brief comparison of the different models, and in particular with Λ CDM, is now in order. At early times, all models exhibit identical behaviour; the same is true once the cosmological constant has attained its final constant value, at which point they all effectively reduce to Λ CDM. Distinctive features arise only during the transition phase and are primarily associated with the manner and smoothness of the evolution.

In order to perform a meaningful comparison among the models, it is necessary to specify the parameters that characterise each of them. The procedure adopted for this purpose is outlined as follows. We begin by specifying the general quantities employed in all numerical simulations. Following Ref. [46] and adopting *Planck 2018* data, we fix the Λ CDM parameters to $H_{0,\Lambda\text{CDM}} = 67.29 \text{ km s}^{-1} \text{ Mpc}^{-1}$, $\Omega_{m0,\Lambda\text{CDM}} = 0.3125$, $\Omega_{r0,\Lambda\text{CDM}} = 9 \times 10^{-5}$, and $\Omega_{d,\Lambda\text{CDM}} = 1 - \Omega_{m0,\Lambda\text{CDM}} - \Omega_{r0,\Lambda\text{CDM}}$. For the sign-switching models, we instead adopt the parameter values obtained in the same work for the abrupt sign-switching scenario, denoted as Λ_s CDM, namely $H_0 = 70.22 \text{ km s}^{-1} \text{ Mpc}^{-1}$, $\Omega_{m0} = 0.2900$, $\Omega_{r0} = 9 \times 10^{-5}$, and $\Omega_{d0} = 1 - \Omega_{m0} - \Omega_{r0}$.

Turning to the characteristic parameters of each model, we fix the sign-switching redshift of model (A) to $z_{\dagger,s} = 1.7$, in agreement with Refs. [45–47, 55]. For model (B), we adopt the same sign-switching redshift, $z_{\dagger,l} = 1.7$, to enable a direct comparison. Assuming a rapid transition, we set the step width to $\Delta z = 0.1$, with the transition beginning at $z_{i,l} = 2.7$ and ending at $z_{f,l} = 0.7$, in accordance with Eq. (4). In model (C), the additional parameters are chosen such that the sign-switching occurs at a comparable redshift and over a transition interval of similar duration. Finally, for model (D), we fix the sign-switching redshift to the same value as in models (A) and (B), while selecting a transition speed comparable to that of model (C) and to the previously studied Λ_s VCDM scenario [50]. For clarity, we summarise the parameter choices as follows: model (A) is characterised by $z_{\dagger,s} = 1.7$; model (B) by $z_{\dagger,l} = 1.7$, and $\Delta z = 0.1$; model (C) by $z_{i,ss} = 2.7$ and $z_{f,ss} = 1$; and model (D) by $\eta = 10$ and $z_{\dagger,e} = 1.7$.

These models can be naturally divided into two distinct classes. The first class comprises models (A) and (B), which display discontinuous behaviour across their defining features. This is evident in both the Hubble parameter $H(z)$ and the EoS parameter, as illustrated in Fig. 1. While the piecewise-constant nature of the DE density simplifies the description of several quantities—since the EoS parameter remains fixed and DE perturbations are absent—the abrupt variations in the DE density give rise to sudden-type singularities [48, 64]. The second class includes models (C) and (D), which instead exhibit fully continuous dynamics. In these scenarios, the Hubble parameter evolves smoothly and the EoS parameter becomes time-dependent. Such variations are expected to play a more prominent role in the cosmographic analysis presented in the following section.

When introducing the models, we noted that all of them exhibit a divergence at the sign-switching point, which arises from the vanishing of the DE density at that instant. Since the EoS parameter is defined as $w_d = p_d/\rho_d$, it necessarily diverges when $\rho_d \rightarrow 0$. This feature is common to all sign-switching models. Nevertheless, as shown in Fig. 1, the total equation-of-state parameter remains well defined throughout the entire evolution. For all sign-switching scenarios, the total EoS parameter exceeds the Λ CDM value prior to the sign change and becomes slightly smaller afterwards. In particular, for the two continuous models, an oscillatory behaviour can be observed, which is expected to become more pronounced in the cosmographic analysis presented

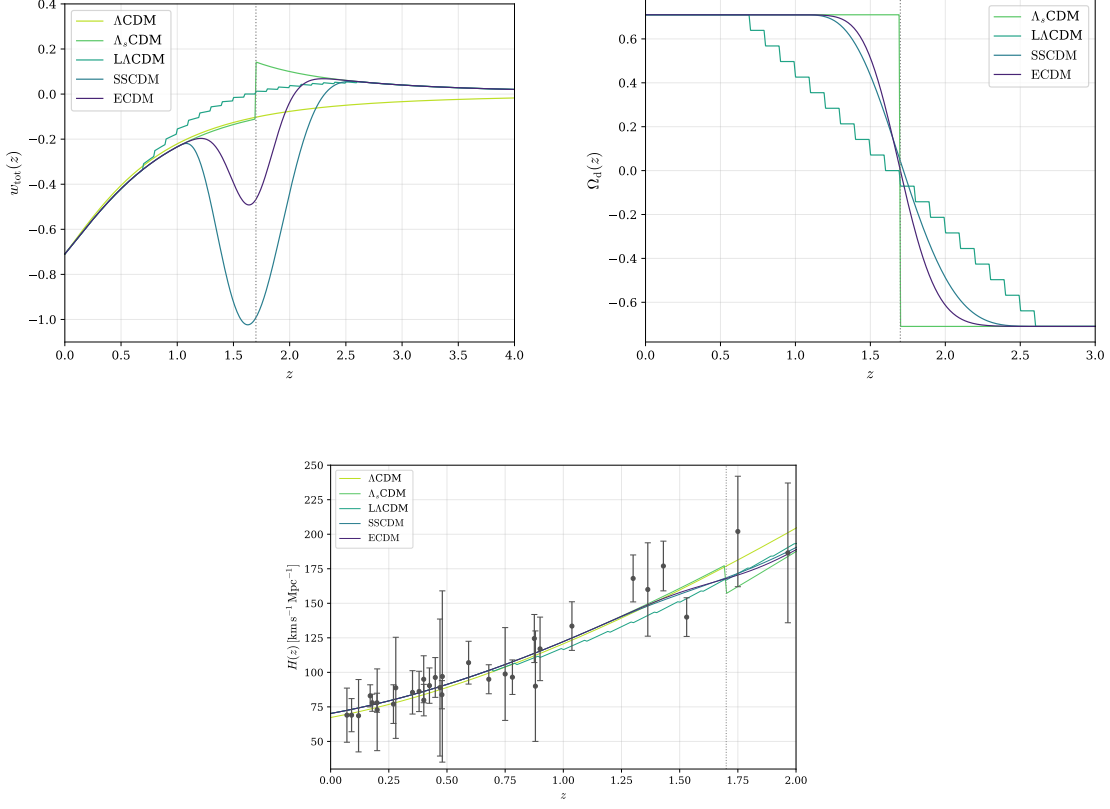


Figure 1: The left figure showcases the total EoS parameter, $w_{\text{tot}}(z)$, against redshift. The right figure showcases the evolution of DE energy density. The bottom figures showcases $H(z)$ in units of km/s/Mpc against redshift. The the error bars were obtained from Ref. [66]. The vertical black line denotes the sign-switching redshift for the DE density.

in the following section.

3. Cosmography

A convenient way to contrast the models discussed above is through a cosmographic analysis [67–69]. This approach is particularly well suited for comparative studies, as it allows one to characterise different cosmological scenarios in terms of a common set of observable parameters.

Within this framework, the scale factor is expanded as a Taylor series around its present-day value a_0 , namely

$$a(t) = a_0 \left[1 + \sum_{n=1}^{\infty} \frac{A_n(t_0)}{n!} [H_0(t - t_0)]^n \right], \quad (10)$$

where t_0 denotes the present cosmic time and H_0 is the Hubble parameter evaluated today. The coefficients of this expansion define the cosmographic parameters A_n , which are given by

$$A_n \equiv \frac{a^{(n)}}{aH^n}, \quad n \in \mathbb{N}, \quad (11)$$

with $a^{(n)}$ representing the n -th derivative of the scale factor with respect to cosmic time.

Several of these parameters have acquired standard names in the literature due to their direct physical interpretation. In particular, the second-order parameter is related to the deceleration parameter, $q = -A_2$, while higher-order terms define the jerk, $j = A_3$, the snap, $s = A_4$, and the lerk, $l = A_5$. These quantities will play a central role in the comparison of the different sign-switching models discussed in this work.

3.1 Cosmographic parameters

In this section, we focus on the behaviour of the cosmographic parameters at low redshift. In Ref. [64], we derived the analytical expressions of these parameters up to the lerk and showed that, for the continuous transition models, higher-order derivatives of the scale factor naturally lead to an increasing number of oscillatory features. This behaviour is expected, as successive time derivatives amplify any underlying variation in the expansion history. For clarity of presentation, and due to space limitations, the results are displayed in two separate columns. This choice is particularly motivated by the continuous models, whose cosmographic parameters exhibit larger amplitudes and richer structure compared to the discontinuous cases.

The top-left panel of Fig. 2 illustrates the redshift evolution of the deceleration parameter, $q(z)$, for all the models considered in this work. In the discontinuous scenarios, namely models (A) and (B), the presence of a negative DE density prior to the sign-switching leads to an effective positive pressure. This results in an enhanced deceleration when compared to the standard Λ CDM case. Following the sign change, these models enter an accelerated expansion phase at a redshift slightly later than that of Λ CDM, eventually converging towards the same asymptotic value. The continuous models, (C) and (D), display a qualitatively different behaviour. One of their most distinctive features is the emergence of an additional, intermediate phase of accelerated expansion. As in the discontinuous cases, these models experience a stronger decelerating phase before the transition. However, owing to the rapid yet smooth nature of the transition, the deceleration parameter crosses the threshold $q = 0$, signalling the onset of a new accelerated epoch around $z \sim 1.8$, that is, after the sign-switching of the DE density, in agreement with the results from Ref. [70, 71]. This phase is short-lived: the Universe subsequently returns to a decelerating regime before finally entering the present-day accelerated expansion, where all models ultimately converge.

The top-right panel of Fig. 2 shows the redshift dependence of the jerk parameter, $j(z)$, for all the models analysed here. In the scenarios with a constant DE density, the jerk is largely determined by the present radiation abundance, Ω_{r0} , and consequently remains close to the Λ CDM value, $j(z) = 1$, throughout the low-redshift regime. In contrast, the continuous transition models display the oscillatory features already discussed in the previous section. These oscillations become increasingly pronounced for higher-order derivatives, as expected within a cosmographic framework. Nonetheless, once the transition region is left behind, the jerk parameter in these models also relaxes back towards the standard behaviour, asymptotically approaching $j(z) = 1$.

The middle row of Fig. 2 presents the evolution of the snap parameter, $s(z)$, highlighting distinct behaviours across the different classes of models. The left-middle panel corresponds to scenarios with a constant DE density. In these cases, the snap parameter takes values lower than those of Λ CDM prior to the sign-switching, before converging towards slightly larger values at the present epoch. The right-middle panel displays the behaviour of the continuous models, (C) and

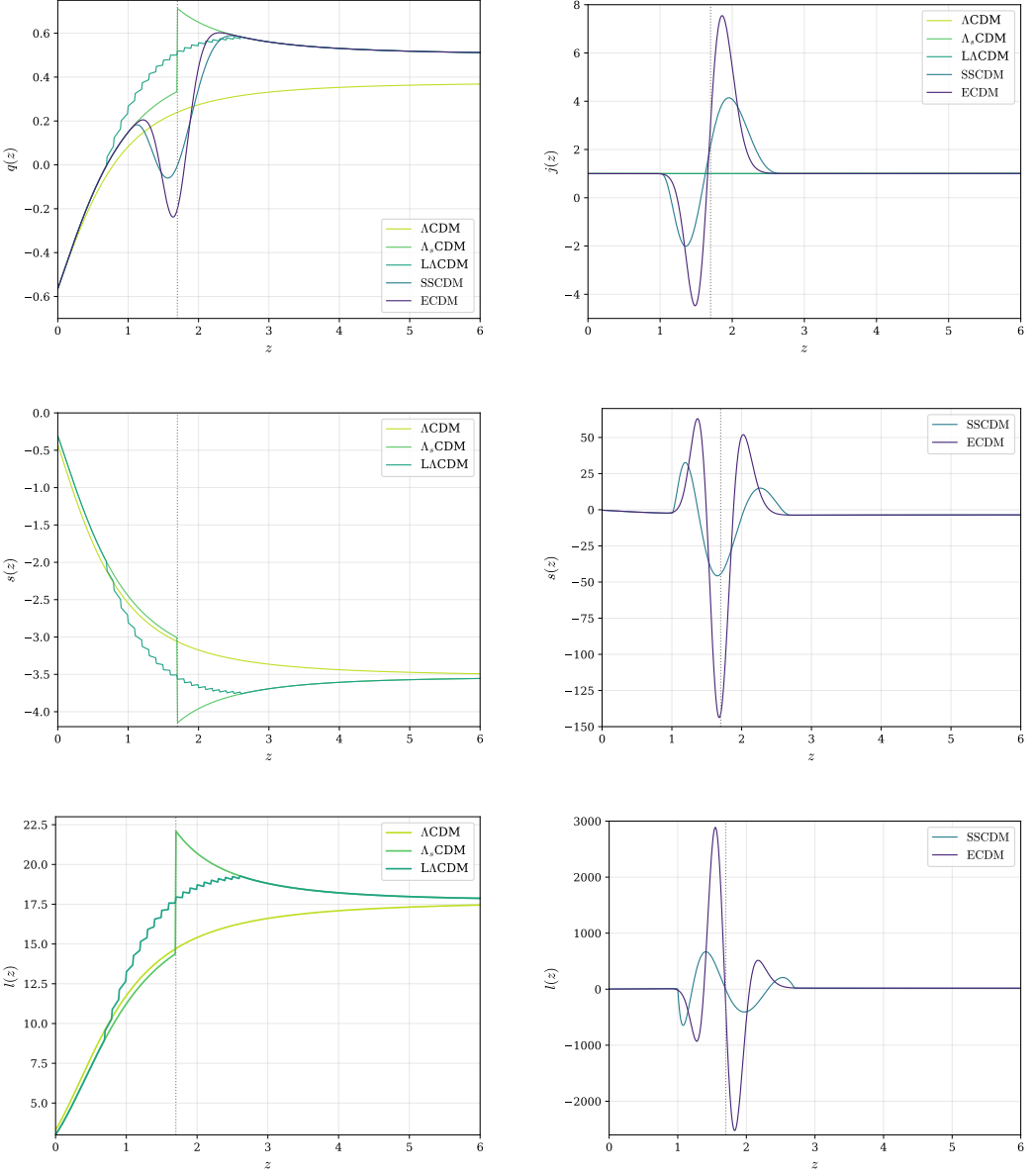


Figure 2: Comparison of the cosmographic parameters $q(z)$, $j(z)$, $s(z)$ and $l(z)$ for the different models. The vertical line denotes the redshift at which the DE density changes sign.

(D), which are characterised by pronounced oscillations in $s(z)$ around the sign-switching redshift. As the DE density gradually settles to its Λ CDM limit, the snap parameter increases and eventually aligns with the behaviour observed in the discontinuous models (A) and (B).

The bottom row of Fig. 2 is devoted to the evolution of the lerk parameter, $l(z)$. The left-bottom panel shows the models with a constant DE density. Before the sign-switching occurs, these scenarios predict lerk values that are systematically larger than those of Λ CDM. After the transition, the trend is reversed, with the models converging towards slightly smaller present-day values. The right-bottom panel displays the continuous transition models, (C) and (D), which again

exhibit the characteristic oscillatory behaviour during the sign-switching epoch. These oscillations, common to all cosmographic parameters in the continuous models, may provide a simple and effective diagnostic for testing their phenomenological viability. In particular, the absence of such oscillatory features—should future observations allow for accurate measurements of higher-order cosmographic parameters—would place strong constraints on, or potentially rule out, this class of models.

4. Cosmological perturbations

Starting from the perturbed FLRW metric in the Newtonian gauge we can compute the perturbed Einstein equations [72–76]. Then following a multi-fluid approach, as done, for example, in [77], and moving to Fourier-space, from the perturbation of the conservation of the energy-momentum tensor we obtain the evolution equation for the fractional energy density perturbation², $\delta_i = \delta\rho_i/\rho_i$, and the peculiar velocity potential, v_i , for each mode and for the different components of the universe:

$$\begin{aligned} (\delta_r)_x &= \frac{4}{3} \left(\frac{k^2}{\mathcal{H}} v_r + 3\Psi_x \right), \\ (v_r)_x &= -\frac{1}{\mathcal{H}} \left(\frac{1}{4} \delta_r + \Psi \right), \\ (\delta_m)_x &= \left(\frac{k^2}{\mathcal{H}} v_r + 3\Psi_x \right), \\ (v_m)_x &= -\left(v_m + \frac{\Psi}{\mathcal{H}} \right), \\ (\delta_d)_x &= (1 + w_d) \left\{ \left[\frac{k^2}{\mathcal{H}} + 9\mathcal{H} \left(c_s^2 - c_a^2 \right) \right] v_d + 3\Psi_x \right\} + 3 \left(w_d - c_s^2 \right) \delta_d, \\ (v_d)_x &= -\frac{1}{\mathcal{H}} \left(\frac{c_s^2}{1 + w_d} \delta_d + \Psi \right) + \left(3c_s^2 - 1 \right) v_d, \end{aligned} \tag{12}$$

and for the metric potential

$$\begin{aligned} \Psi_x + \Psi \left(1 + \frac{k^2}{3\mathcal{H}^2} \right) &= -\frac{1}{2} \delta, \\ \Psi_x + \Psi &= -\frac{3}{2} \mathcal{H} v (1 + w), \\ \Psi_{xx} + \left[3 - \frac{1}{2} (1 + 3w) \right] \Psi_x - 3w\Psi &= \frac{3}{2} \frac{\delta p}{\rho}, \end{aligned} \tag{13}$$

where $\{\}_x$ indicates derivatives with respect to $\ln(a/a_0)$, Ψ denotes the gravitational potential, k is the Fourier wavenumber, and \mathcal{H} is the Hubble parameter expressed in conformal time. For models (A) and (B), perturbations are absent owing to the constant character of their DE density. In the case of Models (C) and (D), DE perturbations are in principle present. However, owing to the assumption of a rapid transition, the DE component remains dynamical only for a very brief

² δ denotes a perturbative variable, not to be confused with the Dirac delta function $\delta(z)$.

interval. Consequently, DE perturbations are expected to remain nearly constant for the majority of the evolution and to exert a negligible influence on the overall dynamics. For this reason, we do not include this component in our analysis.

4.1 Numerical results

In this section, we investigate the evolution of the perturbative variables δ_m , v_m , δ_r and v_r by numerically integrating the coupled system of Eqs. (12) and (13). The integration is performed from deep within the radiation-dominated era, corresponding to $x = -15$ ($z \sim 10^6$), up to the future epoch $x = 2$ ($z = -0.5$). Initial conditions are imposed following the prescription of Ref. [65]. The numerical procedure is repeated for a range of Fourier modes spanning from $k = 0.1 \text{ h Mpc}^{-1}$ down to $k = 3.33 \times 10^{-4} \text{ h Mpc}^{-1}$, allowing us to probe both small- and large-scale perturbations across cosmic time.

4.1.1 Matter perturbations

In Fig. 3, we present the evolution of cosmological perturbations from an initial epoch to a later stage in the Universe's evolution. The four panels depict the progression of the fractional energy density perturbations in matter, δ_m , for the various models under investigation. In each panel, the solid lines denote the outcomes for the respective model, whereas the dotted lines indicate those of the Λ CDM model. Results are shown for six distinct wave numbers, with three qualitatively distinct behaviours depending on their range:

- **Large** $k = 0.1 \text{ h Mpc}^{-1}$ (Purple) and $k = 3.19 \times 10^{-2} \text{ h Mpc}^{-1}$ (Blue).
- **Intermediate** $k = 1.02 \times 10^{-2} \text{ h Mpc}^{-1}$ (Cyan) and $k = 3.27 \times 10^{-3} \text{ h Mpc}^{-1}$ (Green).
- **Small** $k = 1.04 \times 10^{-3} \text{ h Mpc}^{-1}$ (Green-yellow) and $k = 3.33 \times 10^{-4} \text{ h Mpc}^{-1}$ (Yellow).

It is only the smaller modes that showcase a noticeable deviation from Λ CDM, that is, the modes that enter the horizon around the sign-switching. The behaviour is similar and consistent around all models. During the radiation-dominated era, the matter density contrast, δ_m , remains approximately constant for each mode until it enters the horizon. Following horizon entry, gravitational collapse initiates the growth of perturbations, which becomes exponential during the matter-dominated epoch. In the subsequent DE-dominated phase, this growth ceases, and δ_m asymptotically approaches a constant value for each mode. It is also noteworthy that modes with larger wave numbers, k , enter the horizon earlier and, as a result, attain higher values of δ_m throughout cosmic evolution.

4.1.2 Gravitational potential

In Fig. 4, we show the evolution of the gravitational potential, normalised to its initial value, Ψ/Ψ_i , for each model in comparison with Λ CDM. We consider the same wave modes as in the previous figures. For the sign-switching models, the evolution of the gravitational potential closely follows that of Λ CDM at all times, except in the vicinity of the sign transition. As the matter-dominated era draws to a close and the DE component becomes dynamically relevant, the negative DE density exerts a significant influence on the evolution, an effect that persists until the transition is completed and the DE density reaches its present value. In Ref. [65], we investigated the

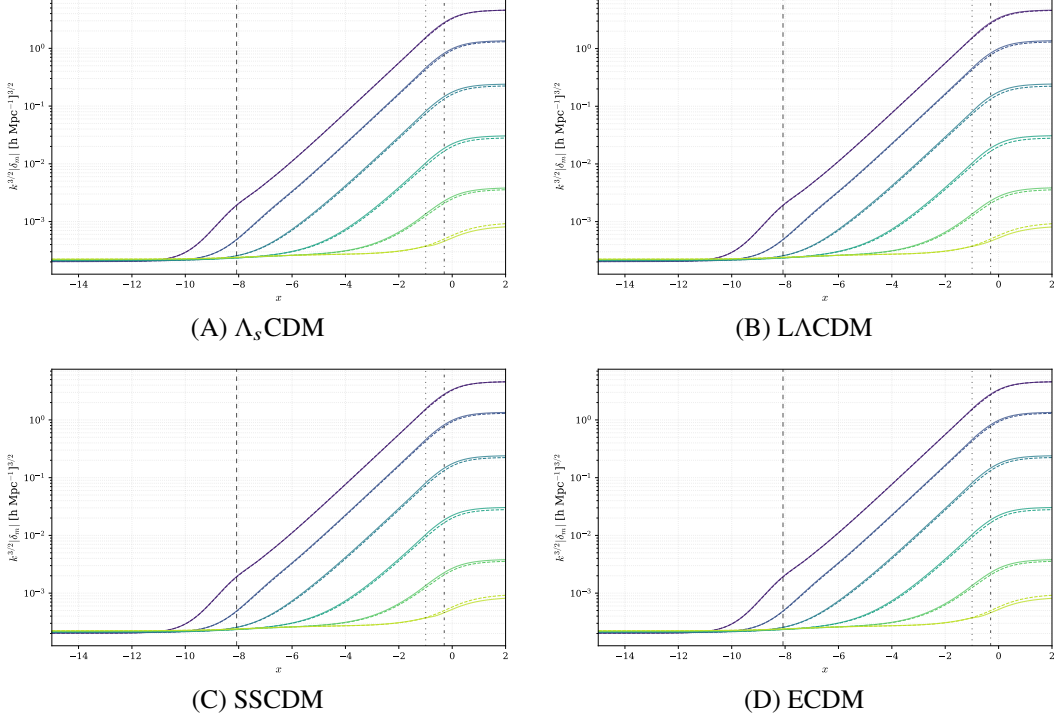


Figure 3: Evolution of fractional energy density perturbations in matter, δ_m , for all sign-switching models (continuous lines) compared against Λ CDM (dashed lines). Each colour corresponds to a different Fourier mode: $k = 3.33 \times 10^{-4} \text{ h Mpc}^{-1}$ (Yellow), $k = 1.04 \times 10^{-3} \text{ h Mpc}^{-1}$ (Green-yellow), $k = 3.27 \times 10^{-3} \text{ h Mpc}^{-1}$ (Green), $k = 1.02 \times 10^{-2} \text{ h Mpc}^{-1}$ (Cyan), $k = 3.19 \times 10^{-2} \text{ h Mpc}^{-1}$ (Blue), $k = 0.1 \text{ h Mpc}^{-1}$ (Purple). The dashed left vertical line indicates the radiation-matter equality, the right one the matter-DE equality, and the dotted vertical line between them corresponds to the sign-switching redshift.

evolution from the distant past ($z \sim 10^6$) to the far future ($z \sim -0.99$); however, in this proceedings contribution we only show the epoch during which the transition from negative to positive DE density occurs, as this is when the models exhibit the largest deviations from Λ CDM.

- **Large k :** The largest modes enter the horizon earliest, during the radiation-dominated era, and consequently experience the strongest suppression. They then settle into an almost constant configuration throughout the matter-dominated epoch. Around the epoch of the sign transition, a mild departure from the Λ CDM evolution becomes apparent, manifesting as a temporary enhancement sourced by the positive DE pressure prior to the transition. Once the sign change is completed, the potential undergoes a further period of decay over a timescale of a few e-folds, before converging towards a small residual constant value in the future.
- **Intermediate k :** The gravitational potential undergoes a brief decay around radiation–matter equality, after which it settles onto a plateau. Subsequently, in a manner analogous to the larger-scale modes, it exhibits an enhancement relative to Λ CDM as the sign-switching epoch is approached, followed by a phase of decay. Notably, the peak associated with the sign transition is more pronounced for these modes than for the larger ones.

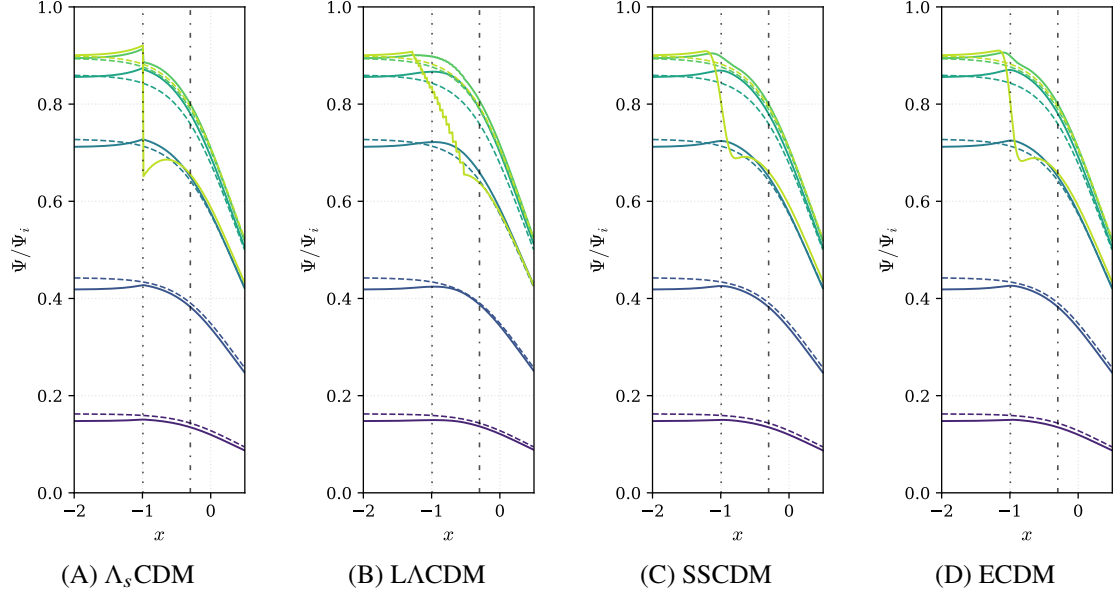


Figure 4: Gravitational potential Ψ/Ψ_i , for all sign-switching models (continuous lines) compared against Λ CDM (dashed lines). Each colour corresponds to a different Fourier mode: $k = 3.33 \times 10^{-4} \text{ h Mpc}^{-1}$ (Yellow), $k = 1.04 \times 10^{-3} \text{ h Mpc}^{-1}$ (Green-yellow), $k = 3.27 \times 10^{-3} \text{ h Mpc}^{-1}$ (Green), $k = 1.02 \times 10^{-2} \text{ h Mpc}^{-1}$ (Cyan), $k = 3.19 \times 10^{-2} \text{ h Mpc}^{-1}$ (Blue), $k = 0.1 \text{ h Mpc}^{-1}$ (Purple). The dashed right vertical line indicates the matter-DE equality, and the dotted left vertical line corresponds to the sign-switching redshift.

- **Small k :** As in the intermediate case, the modes experience a mild suppression around radiation–matter equality, after which a plateau is established. The most distinctive features arise as the sign-switching epoch is approached, where the behaviour becomes strongly model dependent. This is illustrated in Figs. 4A and 4B: model (A) undergoes a sharp drop at the transition, while model (B) exhibits a smoother evolution as a consequence of its step-like structure. In contrast, Models (C) and (D), shown in Fig. 4, are characterised by a rapid but smooth decay associated with the continuous evolution of the DE density. At later times, the evolution converges towards the same values as the ones observed in the previous scenarios.

4.1.3 $f\sigma_8$ distribution

One of the key quantities characterising structure formation is the growth rate of matter perturbations, defined as [77, 78]

$$f = \frac{d \ln \delta_m}{d \ln a}, \quad (14)$$

where δ_m denotes the fractional matter overdensity for a given Fourier mode. In observations, however, the combination $f\sigma_8$ is commonly used rather than f alone. Here, σ_8 represents the root-mean-square of matter fluctuations within spheres of radius $8 \text{ h}^{-1} \text{ Mpc}$ and serves as the normalisation for the matter power spectrum. The advantage of considering $f\sigma_8$ lies in reducing the degeneracy between the linear galaxy bias b , which relates the dark matter perturbations to the observed galaxy density fluctuations, and σ_8 , allowing for a more direct comparison with galaxy surveys.

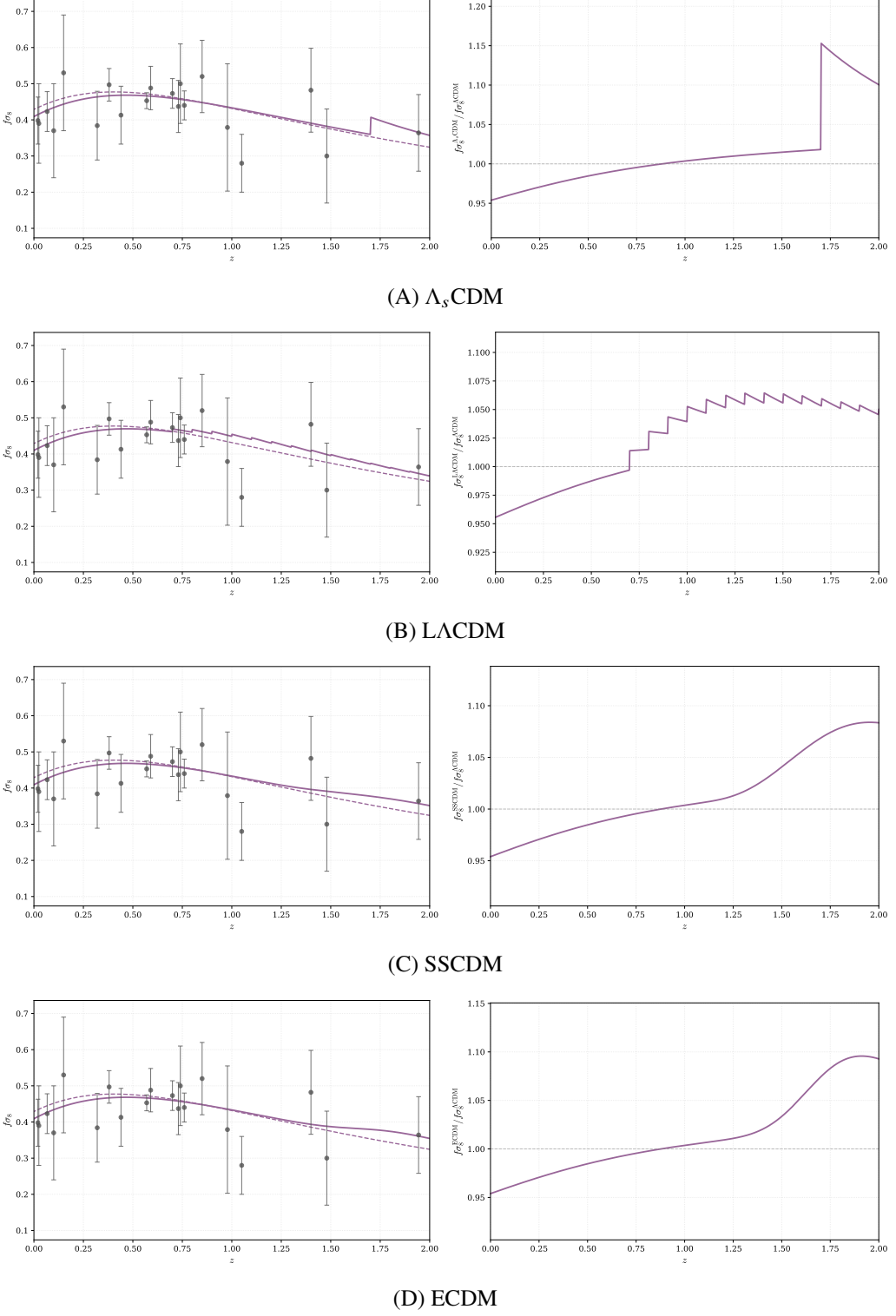


Figure 5: The left columns corresponds to the evolution of $f\sigma_8$ for redshift between $z = 0$ and $z = 2$ against the data points of Ref. [79]. The continuous lines correspond to the respective models of study while the dashed ones to Λ CDM. The right column corresponds to the ratio of $f\sigma_8$ of each models against Λ CDM.

The evolution of σ_8 is computed as

$$\sigma_8(z, k_{\sigma_8}) = \sigma_8(0, k_{\sigma_8}) \frac{\delta_m(z, k_{\sigma_8})}{\delta_m(0, k_{\sigma_8})}, \quad (15)$$

with $k_{\sigma_8} = 0.125 \text{ h Mpc}^{-1}$ corresponding to the physical $8 \text{ h}^{-1} \text{Mpc}$ scale. We solve Eqs. (12) and (13), together with (14) and (15), to obtain the evolution of $f\sigma_8$ for each model. All computations adopt the Planck 2018 normalisation, $\sigma_8(0, k_{\sigma_8}) = 0.8120$ [80], and the results are compared both with the standard ΛCDM predictions and with observational data from Ref. [79].

Figure 5 summarises these results, showing the evolution of $f\sigma_8$ relative to ΛCDM across $z \in [0, 2]$ for all four models. Predictions of our models are displayed in continuous violet, while ΛCDM is shown in dashed lines. We find that all scenarios remain within the observational uncertainties throughout most of the redshift range. Notably, all four models provide an improved match to the highest and lowest redshift measurements from quasar and EBOSS data [79], lying closer to the observed value than the ΛCDM curve.

Panels 5A and 5B illustrate the difference between a single-step transition and a generalised ladder-step scenario, respectively. In the continuous-transition models (C) and (D) (panels 5C and 5D), $f\sigma_8$ evolves from slightly elevated values toward the ΛCDM expectation as the DE density transitions from negative to positive. In all four models, an enhancement of structure formation is apparent in the vicinity of the sign-switching epoch, reflecting the temporary influence of negative DE density on matter clustering. In general, the same behaviour is apparent for all four models: a suppression of $f\sigma_8$ at redshifts close to the present epoch, when the DE density becomes larger than in ΛCDM , and an enhancement at higher redshift values due to the effect of the positive DE pressure.

5. Conclusions

Motivated by scenarios in which the cosmological constant is allowed to change sign, we have investigated a set of DE models extending the $\Lambda_s\text{CDM}$ framework. These include a phenomenological ladder-step construction (Model (B), or L ΛCDM) and two dynamically evolving realisations, SSCDM and ECDM (Models (C) and (D)), in which the transition from negative to positive DE density is implemented smoothly. Together, these models provide a unified setting in which abrupt and continuous sign changes of the DE sector can be studied within a consistent cosmological framework.

At the level of the homogeneous background, we explored the expansion history using both analytical and numerical techniques, focusing on the evolution of the Hubble parameter and on cosmographic diagnostics. The models with discontinuous transitions display sharp features in the deceleration and higher-order kinematic parameters, whereas the smooth-transition scenarios are characterised by regular and continuous behaviour across the entire redshift range.

We then extended the analysis to linear perturbations in order to assess the implications for structure formation. Matter density perturbations remain close to their ΛCDM counterparts, with only small departures across all cases. More pronounced differences appear in the evolution of the gravitational potential around the epochs of matter-DE equality and sign transition. In particular, discontinuous models give rise to abrupt variations, while the continuous scenarios exhibit a rapid

but smooth decay. This behaviour is reflected in late-time observables, where a modest enhancement of the growth-related quantity $f\sigma_8$ is found relative to Λ CDM, especially in the smoothly evolving models, where the negative DE phase temporarily amplifies clustering.

Taken together, our results show that sign-switching models yield a viable background expansion history while simultaneously inducing subtle, yet potentially testable, deviations in the growth of cosmic structures. Although the predicted effects are moderate, they lead to a distinctive phenomenology that motivates a direct confrontation with observations. A first dedicated statistical analysis of the models introduced in [64] and reviewed here, using current cosmological datasets, was performed in [70], where their observational viability was assessed. That study shows that sign-switching dark energy models constitute a consistent extension of Λ CDM, capable of alleviating existing cosmological tensions while producing characteristic dynamical signatures.

Acknowledgements

M. B.-L. is supported by the Basque Foundation of Science Ikerbasque. Our work is supported by the Spanish Grant PID2023-149016NB-I00 funded by (MCIN/AEI/10.13039/501100011033 and by “ERDF A way of making Europe”). The authors acknowledge the contribution of the COST Action CA21136 “Addressing observational tensions in cosmology with systematics and fundamental physics (CosmoVerse)”. This work is also supported by the Basque government Grant No. IT1628-22 (Spain) and in particular B. I. U. is funded through that Grant.

References

- [1] SUPERNOVA SEARCH TEAM collaboration, *Observational evidence from supernovae for an accelerating universe and a cosmological constant*, *Astron. J.* **116** (1998) 1009 [[astro-ph/9805201](#)].
- [2] E. Di Valentino, O. Mena, S. Pan, L. Visinelli, W. Yang, A. Melchiorri et al., *In the realm of the Hubble tension—a review of solutions*, *Class. Quant. Grav.* **38** (2021) 153001 [[2103.01183](#)].
- [3] V. Poulin, T.L. Smith, T. Karwal and M. Kamionkowski, *Early Dark Energy Can Resolve The Hubble Tension*, *Phys. Rev. Lett.* **122** (2019) 221301 [[1811.04083](#)].
- [4] M. Kamionkowski and A.G. Riess, *The Hubble Tension and Early Dark Energy*, *Ann. Rev. Nucl. Part. Sci.* **73** (2023) 153 [[2211.04492](#)].
- [5] L. Perivolaropoulos and F. Skara, *Challenges for Λ CDM: An update*, *New Astron. Rev.* **95** (2022) 101659 [[2105.05208](#)].
- [6] E. Abdalla et al., *Cosmology intertwined: A review of the particle physics, astrophysics, and cosmology associated with the cosmological tensions and anomalies*, *JHEAp* **34** (2022) 49 [[2203.06142](#)].

[7] K. Bamba, S. Capozziello, S. Nojiri and S.D. Odintsov, *Dark energy cosmology: the equivalent description via different theoretical models and cosmography tests*, *Astrophys. Space Sci.* **342** (2012) 155 [[1205.3421](#)].

[8] CosmoVERSE collaboration, E. Di Valentino et al., *The CosmoVerse White Paper: Addressing observational tensions in cosmology with systematics and fundamental physics*, 4, 2025.

[9] G. Ye and Y.-S. Piao, *Is the Hubble tension a hint of AdS phase around recombination?*, *Phys. Rev. D* **101** (2020) 083507 [[2001.02451](#)].

[10] G. Ye and Y.-S. Piao, *T_0 censorship of early dark energy and AdS vacua*, *Phys. Rev. D* **102** (2020) 083523 [[2008.10832](#)].

[11] G. Ye, J. Zhang and Y.-S. Piao, *Alleviating both H_0 and S_8 tensions: Early dark energy lifts the CMB-lockdown on ultralight axion*, *Phys. Lett. B* **839** (2023) 137770 [[2107.13391](#)].

[12] F. Niedermann and M.S. Sloth, *New early dark energy*, *Phys. Rev. D* **103** (2021) L041303 [[1910.10739](#)].

[13] J.S. Cruz, F. Niedermann and M.S. Sloth, *Cold New Early Dark Energy pulls the trigger on the H_0 and S_8 tensions: a simultaneous solution to both tensions without new ingredients*, *JCAP* **11** (2023) 033 [[2305.08895](#)].

[14] F. Niedermann and M.S. Sloth, *New Early Dark Energy as a solution to the H_0 and S_8 tensions*, 7, 2023.

[15] M. Bouhmadi-López and A. Ferrera, *Crossing the cosmological constant line in a dilatonic brane-world model with and without curvature corrections*, *JCAP* **10** (2008) 011 [[0807.4678](#)].

[16] E. Di Valentino, A. Mukherjee and A.A. Sen, *Dark Energy with Phantom Crossing and the H_0 Tension*, *Entropy* **23** (2021) 404 [[2005.12587](#)].

[17] G. Alestas, L. Kazantzidis and L. Perivolaropoulos, *H_0 tension, phantom dark energy, and cosmological parameter degeneracies*, *Phys. Rev. D* **101** (2020) 123516 [[2004.08363](#)].

[18] S.A. Adil, O. Akarsu, E. Di Valentino, R.C. Nunes, E. Özülker, A.A. Sen et al., *Omnipotent dark energy: A phenomenological answer to the Hubble tension*, *Phys. Rev. D* **109** (2024) 023527 [[2306.08046](#)].

[19] J. Morais, M. Bouhmadi-López, K. Sravan Kumar, J. Marto and Y. Tavakoli, *Interacting 3-form dark energy models: distinguishing interactions and avoiding the Little Sibling of the Big Rip*, *Phys. Dark Univ.* **15** (2017) 7 [[1608.01679](#)].

[20] S. Kumar and R.C. Nunes, *Echo of interactions in the dark sector*, *Phys. Rev. D* **96** (2017) 103511 [[1702.02143](#)].

[21] R.C. Nunes, S. Vagnozzi, S. Kumar, E. Di Valentino and O. Mena, *New tests of dark sector interactions from the full-shape galaxy power spectrum*, *Phys. Rev. D* **105** (2022) 123506 [[2203.08093](#)].

[22] M. Kamionkowski, J. Pradler and D.G.E. Walker, *Dark energy from the string axiverse*, *Phys. Rev. Lett.* **113** (2014) 251302 [[1409.0549](#)].

[23] R. Emami, D. Grin, J. Pradler, A. Raccanelli and M. Kamionkowski, *Cosmological tests of an axiverse-inspired quintessence field*, *Phys. Rev. D* **93** (2016) 123005 [[1603.04851](#)].

[24] H.-W. Chiang, C.G. Boiza and M. Bouhmadi-López, *Observational constraints on generalised axion-like potentials for the late Universe*, *JCAP* **08** (2025) 064 [[2503.04898](#)].

[25] T.P. Sotiriou and V. Faraoni, *$f(R)$ Theories Of Gravity*, *Rev. Mod. Phys.* **82** (2010) 451 [[0805.1726](#)].

[26] A. De Felice and S. Tsujikawa, *$f(R)$ theories*, *Living Rev. Rel.* **13** (2010) 3 [[1002.4928](#)].

[27] S. Nojiri and S.D. Odintsov, *Unified cosmic history in modified gravity: from $F(R)$ theory to Lorentz non-invariant models*, *Phys. Rept.* **505** (2011) 59 [[1011.0544](#)].

[28] S. Nojiri, S.D. Odintsov and V.K. Oikonomou, *Modified Gravity Theories on a Nutshell: Inflation, Bounce and Late-time Evolution*, *Phys. Rept.* **692** (2017) 1 [[1705.11098](#)].

[29] G.R. Bengochea and R. Ferraro, *Dark torsion as the cosmic speed-up*, *Phys. Rev. D* **79** (2009) 124019 [[0812.1205](#)].

[30] R. Ferraro and F. Fiorini, *Modified teleparallel gravity: Inflation without inflaton*, *Phys. Rev. D* **75** (2007) 084031 [[gr-qc/0610067](#)].

[31] Y.-F. Cai, S. Capozziello, M. De Laurentis and E.N. Saridakis, *$f(T)$ teleparallel gravity and cosmology*, *Rept. Prog. Phys.* **79** (2016) 106901 [[1511.07586](#)].

[32] M. Bouhmadi-López, C.G. Boiza, M. Petronikolou and E.N. Saridakis, *Modified Teleparallel $f(T)$ Gravity, DESI BAO and the H_0 Tension*, 1, 2026.

[33] T. Harko, F.S.N. Lobo, S. Nojiri and S.D. Odintsov, *$f(R, T)$ gravity*, *Phys. Rev. D* **84** (2011) 024020 [[1104.2669](#)].

[34] S. Nojiri and S.D. Odintsov, *Gravity assisted dark energy dominance and cosmic acceleration*, *Phys. Lett. B* **599** (2004) 137 [[astro-ph/0403622](#)].

[35] J. Beltrán Jiménez, L. Heisenberg and T.S. Koivisto, *Teleparallel Palatini theories*, *JCAP* **08** (2018) 039 [[1803.10185](#)].

[36] J. Beltrán Jiménez, L. Heisenberg, T.S. Koivisto and S. Pekar, *Cosmology in $f(Q)$ geometry*, *Phys. Rev. D* **101** (2020) 103507 [[1906.10027](#)].

[37] I. Ayuso, R. Lazkoz and V. Salzano, *Observational constraints on cosmological solutions of $f(Q)$ theories*, *Phys. Rev. D* **103** (2021) 063505 [[2012.00046](#)].

[38] C.G. Boiza, M. Petronikolou, M. Bouhmadi-López and E.N. Saridakis, *Addressing H_0 and S_8 tensions within $f(Q)$ cosmology*, *JCAP* **12** (2025) 011 [[2505.18264](#)].

[39] I. Ayuso, M. Bouhmadi-López, C.-Y. Chen, X.Y. Chew, K. Dialetopoulos and Y.C. Ong, *Insights in $f(Q)$ cosmology: the relevance of the connection*, 6, 2025.

[40] T. Kobayashi, *Horndeski theory and beyond: a review*, *Rept. Prog. Phys.* **82** (2019) 086901 [[1901.07183](#)].

[41] C. Deffayet, O. Pujolas, I. Sawicki and A. Vikman, *Imperfect Dark Energy from Kinetic Gravity Braiding*, *JCAP* **10** (2010) 026 [[1008.0048](#)].

[42] O. Pujolas, I. Sawicki and A. Vikman, *The Imperfect Fluid behind Kinetic Gravity Braiding*, *JHEP* **11** (2011) 156 [[1103.5360](#)].

[43] T. Borislavov Vasilev, M. Bouhmadi-López and P. Martín-Moruno, *Phantom attractors in kinetic gravity braiding theories: a dynamical system approach*, *JCAP* **06** (2023) 026 [[2212.02547](#)].

[44] T. Borislavov Vasilev, M. Bouhmadi-López and P. Martín-Moruno, *Dark energy with a shift-symmetric scalar field: Obstacles, loophole hunting and dead ends*, *Phys. Dark Univ.* **46** (2024) 101679 [[2406.12576](#)].

[45] O. Akarsu, S. Kumar, E. Özülker and J.A. Vazquez, *Relaxing cosmological tensions with a sign switching cosmological constant*, *Phys. Rev. D* **104** (2021) 123512 [[2108.09239](#)].

[46] O. Akarsu, S. Kumar, E. Özülker, J.A. Vazquez and A. Yadav, *Relaxing cosmological tensions with a sign switching cosmological constant: Improved results with Planck, BAO, and Pantheon data*, *Phys. Rev. D* **108** (2023) 023513 [[2211.05742](#)].

[47] O. Akarsu, E. Di Valentino, S. Kumar, R.C. Nunes, J.A. Vazquez and A. Yadav, Λ_s CDM model: A promising scenario for alleviation of cosmological tensions, 7, 2023.

[48] E.A. Paraskevas, A. Cam, L. Perivolaropoulos and O. Akarsu, *Transition dynamics in the Λ_s CDM model: Implications for bound cosmic structures*, *Phys. Rev. D* **109** (2024) 103522 [[2402.05908](#)].

[49] Ö. Akarsu, A. De Felice, E. Di Valentino, S. Kumar, R.C. Nunes, E. Özülker et al., Λ_s CDM cosmology from a type-II minimally modified gravity, *Mon. Not. Roy. Astron. Soc.* **546** (2026) staf2276 [[2402.07716](#)].

[50] O. Akarsu, A. De Felice, E. Di Valentino, S. Kumar, R.C. Nunes, E. Özülker et al., *Cosmological constraints on Λ_s CDM scenario in a type II minimally modified gravity*, *Phys. Rev. D* **110** (2024) 103527 [[2406.07526](#)].

[51] O. Akarsu, B. Buldu, A. De Felice, N. Katircı and N.M. Uzun, *Unexplored regions in teleparallel $f(T)$ gravity: Sign-changing dark energy density*, *Phys. Rev. D* **112** (2025) 083532 [[2410.23068](#)].

[52] M.S. Souza, A.M. Barcelos, R.C. Nunes, O. Akarsu and S. Kumar, *Mapping the Λ_s CDM Scenario to $f(T)$ Modified Gravity: Effects on Structure Growth Rate*, *Universe* **11** (2025) 2 [2501.18031].

[53] O. Akarsu, L. Perivolaropoulos, A. Tsikoudoura, A.E. Yükselci and A. Zhuk, *Dynamical dark energy with AdS-to-dS and dS-to-dS transitions: Implications for the H_0 tension*, 2, 2025.

[54] Ö. Akarsu, A. Çam, E.A. Paraskevas and L. Perivolaropoulos, *Linear matter density perturbations in the Λ_s CDM model: Examining growth dynamics and addressing the S_8 tension*, *JCAP* **08** (2025) 089 [2502.20384].

[55] L.A. Escamilla, O. Akarsu, E. Di Valentino, E. Özülker and J.A. Vazquez, *Exploring the Growth-Index (γ) Tension with Λ_s CDM*, 3, 2025.

[56] O. Akarsu, M. Eingorn, L. Perivolaropoulos, A.E. Yükselci and A. Zhuk, *Dynamical dark energy with AdS-dS transitions vs. Baryon Acoustic Oscillations at $z = 2.3\text{-}2.4$* , 4, 2025.

[57] O. Akarsu, E. Di Valentino, J. Vyskočil, E. Yilmaz, A.E. Yukselci and A. Zhuk, *Nonlinear Matter Power Spectrum from relativistic N-body Simulations: Λ_s CDM versus Λ CDM*, 10, 2025.

[58] P. Ghafari, M. Najafi, M. Ghodsi Yengejeh, E. Özülker, E. Di Valentino and J.T. Firouzjaee, *A Multi-Probe ISW Study of Dark Energy Models with Negative Energy Density: Galaxy Correlations, Lensing Bispectrum, and Planck ISW-Lensing Likelihood*, 12, 2025.

[59] S. Di Gennaro and Y.C. Ong, *Sign Switching Dark Energy from a Running Barrow Entropy*, *Universe* **8** (2022) 541 [2205.09311].

[60] M. Yadav, A. Dixit, A. Pradhan and M.S. Barak, *Empirical validation: Investigating the Λ sCDM model with new DESI BAO observations*, *JHEAp* **49** (2026) 100453 [2509.26049].

[61] O. Akarsu, J.D. Barrow, L.A. Escamilla and J.A. Vazquez, *Graduated dark energy: Observational hints of a spontaneous sign switch in the cosmological constant*, *Phys. Rev. D* **101** (2020) 063528 [1912.08751].

[62] J.M. Maldacena, *The Large N limit of superconformal field theories and supergravity*, *Adv. Theor. Math. Phys.* **2** (1998) 231 [hep-th/9711200].

[63] S. Nojiri, S.D. Odintsov and S. Tsujikawa, *Properties of singularities in (phantom) dark energy universe*, *Phys. Rev. D* **71** (2005) 063004 [hep-th/0501025].

[64] M. Bouhmadi-López and B. Ibarra-Uriondo, *Cosmographic analysis of sign-switching dark energy*, *Phys. Rev. D* **112** (2025) 063559 [2506.12139].

[65] M. Bouhmadi-López and B. Ibarra-Uriondo, *Cosmological perturbations for smooth sign-switching dark energy models*, *Phys. Dark Univ.* **50** (2025) 102129 [2506.18992].

[66] A. Favale, A. Gómez-Valent and M. Migliaccio, *Cosmic chronometers to calibrate the ladders and measure the curvature of the Universe. A model-independent study*, *Mon. Not. Roy. Astron. Soc.* **523** (2023) 3406 [[2301.09591](#)].

[67] M. Visser, *Cosmography: Cosmology without the Einstein equations*, *Gen. Rel. Grav.* **37** (2005) 1541 [[gr-qc/0411131](#)].

[68] C. Cattoen and M. Visser, *The Hubble series: Convergence properties and redshift variables*, *Class. Quant. Grav.* **24** (2007) 5985 [[0710.1887](#)].

[69] S. Capozziello, V.F. Cardone and V. Salzano, *Cosmography of $f(R)$ gravity*, *Phys. Rev. D* **78** (2008) 063504 [[0802.1583](#)].

[70] B. Ibarra-Uriondo and M. Bouhmadi-López, *Sign-Switching Dark Energy: Smooth Transitions with Recent DESI DR2 Observations*, 2, 2026.

[71] Ö. Akarsu, M. Caruana, K.F. Dialektopoulos, L.A. Escamilla, E.O. Kahya and J. Levi Said, *Hints of sign-changing scalar field energy density and a transient acceleration phase at $z \sim 2$ from model-agnostic reconstructions*, 2, 2026.

[72] D. Baumann, *Cosmology: Part III Mathematical Tripos (Lecture notes)*, Cambridge (2012).

[73] R.H. Brandenberger, H. Feldman and V.F. Mukhanov, *Classical and quantum theory of perturbations in inflationary universe models*, in *37th Yamada Conference: Evolution of the Universe and its Observational Quest*, pp. 19–30, 7, 1993 [[astro-ph/9307016](#)].

[74] C.-P. Ma and E. Bertschinger, *Cosmological perturbation theory in the synchronous and conformal Newtonian gauges*, *Astrophys. J.* **455** (1995) 7 [[astro-ph/9506072](#)].

[75] R.H. Brandenberger, *The Early Universe and Observational Cosmology*, Springer Berlin Heidelberg (2004).

[76] K.A. Malik and D. Wands, *Cosmological perturbations*, *Physics Reports* **475** (2009) 1–51.

[77] I. Albaran, M. Bouhmadi-López and J. Morais, *Cosmological perturbations in an effective and genuinely phantom dark energy Universe*, *Phys. Dark Univ.* **16** (2017) 94 [[1611.00392](#)].

[78] A. Balcerzak and T. Denkiewicz, *Density perturbations in a finite scale factor singularity universe*, *Phys. Rev. D* **86** (2012) 023522 [[1202.3280](#)].

[79] F. Avila, A. Bernui, A. Bonilla and R.C. Nunes, *Inferring $S_8(z)$ and $\gamma(z)$ with cosmic growth rate measurements using machine learning*, *Eur. Phys. J. C* **82** (2022) 594 [[2201.07829](#)].

[80] PLANCK collaboration, *Planck 2018 results. VI. Cosmological parameters*, *Astron. Astrophys.* **641** (2020) A6 [[1807.06209](#)].